

Limited-path-length entanglement percolation in quantum complex networks

Martí Cuquet* and John Calsamiglia

Grup de Física Teòrica: Informació i Fenòmens Quàntics, Universitat Autònoma de Barcelona, E-08193 Bellaterra, Barcelona, Spain

(Received 25 November 2010; published 25 March 2011)

We study entanglement distribution in quantum complex networks where nodes are connected by bipartite entangled states. These networks are characterized by a complex structure, which dramatically affects how information is transmitted through them. For pure quantum state links, quantum networks exhibit a remarkable feature absent in classical networks: it is possible to effectively rewire the network by performing local operations on the nodes. We propose a family of such quantum operations that decrease the entanglement percolation threshold of the network and increase the size of the giant connected component. We provide analytic results for complex networks with an arbitrary (uncorrelated) degree distribution. These results are in good agreement with numerical simulations, which also show enhancement in correlated and real-world networks. The proposed quantum preprocessing strategies are not robust in the presence of noise. However, even when the links consist of (noisy) mixed-state links, one can send quantum information through a connecting path with a fidelity that decreases with the path length. In this noisy scenario, complex networks offer a clear advantage over regular lattices, namely, the fact that two arbitrary nodes can be connected through a relatively small number of steps, known as the small-world effect. We calculate the probability that two arbitrary nodes in the network can successfully communicate with a fidelity above a given threshold. This amounts to working out the classical problem of percolation with a limited path length. We find that this probability can be significant even for paths limited to few connections and that the results for standard (unlimited) percolation are soon recovered if the path length exceeds by a finite amount the average path length, which in complex networks generally scales logarithmically with the size of the network.

DOI: [10.1103/PhysRevA.83.032319](https://doi.org/10.1103/PhysRevA.83.032319)

PACS number(s): 03.67.Bg, 89.75.Hc, 64.60.ah

I. INTRODUCTION

Networks permeate all informational structures. They underlie natural, social, and artificial systems where different parties interact, describing the flow of information between them. Differences in the characteristics of such interactions and how they evolve give growth to different types of structures: regular lattices, completely random networks, and, spanning the range between these two, complex networks, which do not have a regular structure but neither are completely random. Quantum information is not an exception, and quantum networks [1] where nodes communicate between them through quantum channels are essential to quantum information processing and distributed applications. One of the key tasks in these networks is the transmission of quantum information between two distant nodes of the network. This task depends not only on the quality of the connections between nodes and on the amount of resources, but also on the underlying structure of the network. Therefore, understanding how structural properties affect the functionality of the network will allow both the design of better network architectures and the modification of existing ones that make feasible communication at farther distances, among a greater number of nodes or in the presence of higher levels of noise.

Two distant nodes in a network may be connected by one path of entangled states (Fig. 1). In this case, long-distance entanglement between two nodes can be established with a probability that decays exponentially with the distance separating the nodes. This problem can be overcome by

quantum repeaters, which create a distant entangled pair of high fidelity [2]. However, this technique requires a number of qubits in each node that scales logarithmically with the distance [3]. More important, though, is that it only considers a one-dimensional connection between the two nodes. These two nodes, however, may be embedded in a more realistic, higher dimensional network. In this case, a higher number of paths may exist, which can help in the communication: with the existence of clusters of nodes connected by entangled states, two distant nodes will be able to establish entanglement between them if they both belong to the same cluster [4]. Entanglement percolation, which makes use of such higher dimensional networks, was first proposed in the honeycomb lattice [5] and later extended to other regular lattices [6,7], to schemes using multipartite entanglement [8] and to noisy networks [9–12]. In Ref. [13], we studied entanglement distribution in a wide class of complex networks with pure-state connections. Complex networks arise in many real scenarios, notably including the most important real-world communication networks, and it is very plausible that they will become relevant in quantum communication architectures too. They offer very rich properties and phenomena. Interesting quantities can be computed requiring only statistical properties. This might seem a limitation but it can represent an advantage: it makes mathematically tractable some problems that are hard or impossible to solve on lattices and provides a minimal description in scenarios where complete knowledge of the system is not available or is hard to obtain.

One of the primary features of networks is the presence, or absence, of a cluster of nodes connected between them (a *connected component*, in graph theory language) whose size is of the order of the size of the network. Such a cluster is called

*marti.cuquet@uab.cat

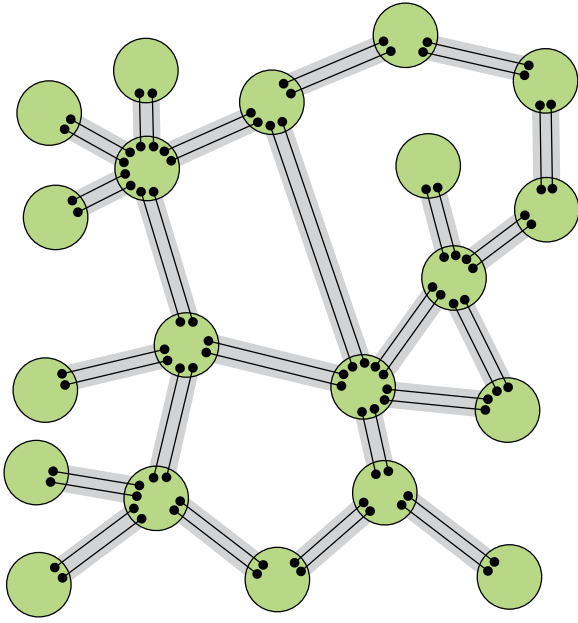


FIG. 1. (Color online) A quantum network. Nodes are large (green) circles. Links between nodes are represented by (gray) bars, each holding a number of bipartite entangled states [narrow (black) lines] shared between nodes.

the giant connected component (GCC), and in the asymptotic limit of infinite-size networks it is defined as the cluster spanning a finite fraction S of nodes of the network. This concept is very closely related to that of a percolating cluster. In bond percolation, for example, edges are occupied with some probability ϕ_1 , thus connecting their end vertices, and vacant with probability $1 - \phi_1$, disconnecting them. Then there exists a percolation threshold ϕ_1^* in this occupation probability: below the threshold, all components are of finite size, while above it there exists one giant connected component whose size is comparable to the network size. This threshold is the critical point of a phase transition, generally of second order, and can be manifested by the divergence of the average component size, which acts like a susceptibility in a magnetic material.

The percolation threshold and the size of the giant connected component, as well as many other properties, strongly depend on the basic structure of the network [14–16] as well as on degree-degree correlations [17,18] and clustering [19]. Therefore, a change in the structure of a network can affect its ability to communicate information. For example, the scale-free topology of the Internet makes it strong—resilient—against the failure of random nodes [20], but not against target attacks directed to its major hubs (nodes with the highest number of neighbors) [21,22]. This relation between the structure of the network and the communication over it can also be exploited to benefit the earlier appearance of the giant cluster and to find architectures that allow communication even in the presence of noise.

In this paper we study the distribution of quantum information over quantum complex networks. We first focus on networks where nodes are connected by bipartite pure entangled states. We propose a transformation of the network that, using only local knowledge, can change the structure of the network and decrease its percolation threshold. We also

calculate how the percolation threshold and the size of the giant component change after the transformation. Then we turn to mixed-state connections between nodes and show that the small-world behavior of many complex networks allows quantum communication above some fidelity bound for finite, but very large, quantum complex networks.

II. RANDOM GRAPHS

A network is naturally represented by a graph G , which is an ordered pair of sets $G = \{V, E\}$. V is the set of vertices (or nodes or points), and E the set of edges (or links or lines), which are pairs of elements of V and represent the connections between them. In this paper we always consider undirected graphs with neither multiple edges (i.e., either zero or one edge between every pair of vertices) nor self-loops. The degree of a vertex, k , is the number of edges emerging from it. A connected component, or cluster, is a subgraph where any two vertices are connected by at least one path of edges and to which no more vertices can be added without losing this property.

Random graphs [23] are ensembles of graphs \mathcal{G} of the same size, with a probability $P(G)$ assigned to every graph G in the ensemble. For any property $O(G)$ of a graph we can calculate its average over the ensemble,

$$\langle O \rangle_G = \sum_{G \in \mathcal{G}} O(G) P(G). \quad (1)$$

However, in most real scenarios, but also in many theoretical models, only a single, large graph is studied. Such graphs are said to be self-averaging if the property we are studying is well characterized by its mean. This happens when the graph is large enough to make fluctuations around the average vanish. For a more detailed discussion about self-averaging, see, for example, Ref. [24] for random graphs and Ref. [25] for the World Wide Web network. We consider this assumption in the following and check its validity numerically in the examples we consider.

One of the basic properties of a graph is the distribution of the probability p_k that a vertex has degree k . There is also a related distribution that will come in handy later and is that of the excess degree: the number of edges k emerging from a vertex reached through another edge and excluding it. This probability can be found easily by considering first the degree of a vertex reached through an edge. Since vertices with a higher degree are easier to reach, this probability is proportional to the degree of the vertex reached, $k p_k / \langle k \rangle$. The excess degree probability r_k is therefore

$$r_k = \frac{(k+1)p_{k+1}}{\langle k \rangle}. \quad (2)$$

Generating functions [26] are a mathematical tool that is very useful when studying properties of graphs described by probability distributions [15]. Among other useful properties, they allow for a straightforward convolution of distributions. Let us introduce them using the degree distribution. The function $g_p(x)$ that generates the distribution $\{p_k\}$ is the power series of x with coefficients equal to the probabilities in the distribution:

$$g_p(x) = \sum_{k \geq 0} p_k x^k. \quad (3)$$

Note that each probability p_k can be recovered from its generating function (3) by taking the k th derivative of $g_p(x)$ at $x = 0$:

$$p_k = \frac{1}{k!} \left. \frac{d^k g_p(x)}{dx^k} \right|_{x=0}. \quad (4)$$

Since the probability distribution is normalized, $\sum_k p_k = 1$, so is its generating function, $g_p(1) = 1$. It is also convergent for $|x| \leq 1$, which is all what we will use here.

The first moment of the distribution p_k , which corresponds to the average degree of the graph $\langle k \rangle$, is equal to the first derivative at $x = 1$:

$$\langle k \rangle = g'_p(1) = \sum_{k \geq 1} k p_k. \quad (5)$$

This allows us to express the generating function for the excess degree distribution, $g_r(x)$, in terms of (3):

$$g_r(x) = \sum_{k \geq 0} r_k x^k = \frac{g'_p(x)}{g'_p(1)}. \quad (6)$$

Higher moments can be similarly found by taking more derivatives. In general, the n th moment is

$$\langle k^n \rangle = \sum_{k \geq 0} k^n p_k = \left[\left(x \frac{d}{dx} \right)^n g_p(x) \right]_{x=1}. \quad (7)$$

Convolution of independent distributions can be obtained by multiplication of their respective generating functions. For example, the total number of edges emerging from n independent vertices (the sum of their degrees) is generated by $[g_p(x)]^n$.

III. NETWORK EXAMPLES

In this paper we calculate properties such as the average component size, the giant connected component size, and the percolation threshold. Analytical results are found for random networks with uncorrelated degree distributions and for the Watts-Strogatz small-world model in the mixed-state scenario. We also discuss several network topologies as concrete examples of our results: the simple Bethe lattice, two networks (Erdős-Rényi and scale free) belonging to the configuration model, the Watts-Strogatz small-world model, and two real-world networks. All of them share a common property known as the “small-world effect”: the average path length, or intervertex distance, scales logarithmically with the size of the network, rather than as a positive power of the size, $N^{1/d}$, as is the case in finite-dimensional networks. Here we present a short description of each of these network models.

Let us start with the simplest network example. The *Bethe lattice* is not a random graph but has some similar properties such as a local tree-like structure and the small-world effect (as long as the degree of its vertices exceeds 2), while at the same time, it remains amenable to analytical study. A Bethe lattice with coordination number k is defined as an infinite regular graph where every vertex has the same degree k and is topologically equivalent to all the others, as shown in Fig. 2. Random regular graphs—graphs where all vertices have a fixed degree but edges are placed randomly—asymptotically

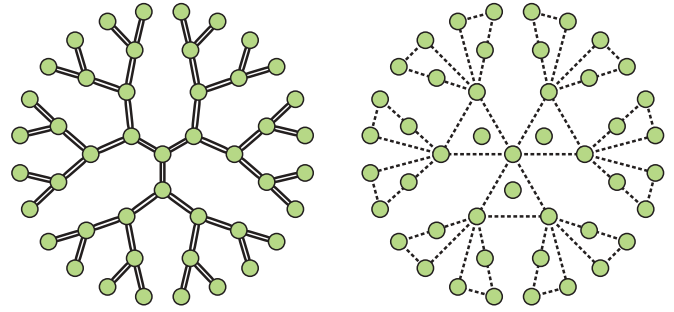


FIG. 2. (Color online) Example of the first five crowns of a Bethe lattice with coordination number $k = 3$. Left: Bethe lattice before q -swap. Right: Same network after applying a 3-swap.

approach Bethe lattices, making them a relevant model where analytical treatment is usually possible.

Erdős-Rényi graphs [27–29] are maximally random graphs with the only constraint $\langle k \rangle = z$. An Erdős-Rényi network with N vertices can be realized by randomly placing $M = Nz/2$ edges or, similarly, by placing an edge between every pair of vertices with probability z/N (also known as the Gilbert model), which is asymptotically equivalent [16]. Figure 3 shows an example of a small Erdős-Rényi network. Their degree distribution is Poissonian, $p_k = e^{-z} z^k / k!$, with generating functions $g_p(x) = g_r(x) = \exp[z(x - 1)]$.

Real-world networks are not Poissonian but typically exhibit a power-law (scale-free) degree distribution, $p_k \sim k^{-\tau}$, characterized by a relatively important number of nodes with a degree much greater than the average. Scale-free networks with $\tau \leq 3$ have a percolation threshold at $\phi_1 = 0$, while for networks with $\tau > 3$ a finite threshold appears. However, in heavy-tailed networks such as these, a cutoff in the degree naturally appears in scenarios where high degrees cannot exist due to, for example, targeted attacks, physical constraints, saturation effects, or finite-size networks. For this reason we consider scale-free networks with an exponential cutoff, $p_k = C k^{-\tau} e^{-k/\kappa}$ (C is a normalizing constant), while the pure scale-free behavior can still be recovered by taking the limit $\kappa \rightarrow \infty$. The cutoff κ strongly affects the network properties, and in particular, networks with $\tau \leq 3$ now have a finite threshold.

Random graphs with uncorrelated degree distributions such as the previous models exhibit a very low level of clustering (also known as transitivity): the likelihood that

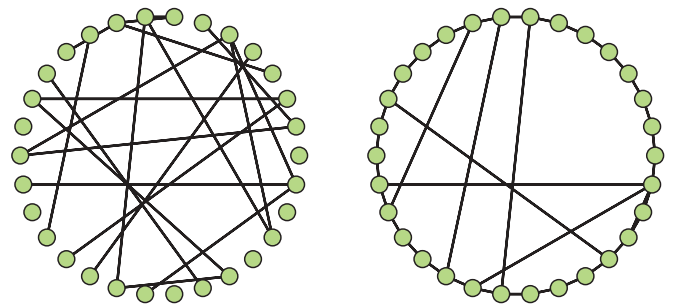


FIG. 3. (Color online) Left: Example of an Erdős-Rényi network with $N = 30$ and $z = 4/3$. Right: Example of a Watts-Strogatz network with $N = 30$ and $\beta = 0.2$.

two neighbors of the same vertex are also neighbors between them. Aside from regular lattices, which have a high level of clustering, there are also many real-world networks with this property. This is especially true for social networks, but also for communication and biological networks. To study this behavior, many models have been proposed, maybe the most studied being the *Watts-Strogatz model* [30]. This model is a random graph with an ordered local structure and a high level of clustering but still with a surprisingly low average path length (see Fig. 3). Here we study a slight modification, also considered in [14]. It is generated by placing N vertices in a one-dimensional ring. Then N additional random edges, called “shortcuts,” are added with probability β , thus giving an average of βN shortcuts.

We also study two real-world networks. The first case represents a real-world scale-free network consisting of *World Wide Web* sites in the nd.edu domain [31]. In this case we introduce an artificial cutoff by neglecting nodes with degree $k \geq 15$, leaving a graph with 142 192 nodes and 170 352 edges. The second real-world example is the *OpenPGP Web of Trust*, a social network representing the trust between OpenPGP users. Without going into much detail, OpenPGP is a standard encryption protocol for securing e-mail communications using public key cryptography. If Alice wants to send a secure message to Bob, she has to use Bob’s public key to encrypt it. The authentication problem arises when Alice cannot verify whether the key she is using is really owned by Bob. A solution to this problem is the Web of Trust, in which every user signs a public key if she trusts it, thus generating a directed graph. To trust a key, usually a user has to meet with the key owner and check that he is really who he claims to be. This social model is thus relevant to quantum communication in the sense that at this point the two users could create a bipartite entangled state and then separate, each keeping one of the parts. By repeatedly doing so between different pairs of users, as in the Web of Trust, a quantum network would be created. Here we use the strongly connected component of the Web of Trust obtained from the Swiss keyserver¹ as of May 25, 2010, containing 41 459 keys and 424 577 signatures. We considered only bidirectional edges, corresponding to users who mutually signed their keys. This leaves an undirected graph with 38 550 keys and 145 388 two-way signatures.

IV. PURE-STATE NETWORKS

We first focus on networks of pure, nonmaximally entangled states, as in [5]. In this case, edges have some probability ϕ_n of being converted into maximally entangled states, depending on the amount of entanglement and the number n of bipartite states per edge. Singlets can then be used for perfect teleportation; that is, they are equivalent to a single-use ideal quantum channel. This strategy can be directly mapped into a bond percolation problem and is thus called *classical entanglement percolation*. There exists, then, a critical probability ϕ_1^* , called the percolation threshold, above which the giant component appears with fractional size $S > 0$.

Above this threshold, any two nodes are able to share maximal entanglement if they both belong to the giant component. This happens with a probability S^2 , which is independent of the distance but strongly depends on the network topology. Hence, for a given type of edge ϕ_n long-distance entanglement will only be possible for networks fulfilling $\phi_n > \phi_1^*$. Remarkably, due to the quantum nature of the connections, it is possible to drastically change the network topology by local actions: a particular measurement is done on qubits within the same node, establishing new connections between neighboring nodes. Thus, a quantum preprocessing of the network can be carried before edges are converted into singlets, so the new structure provides, for example, a better percolation threshold. Moreover, to carry the particular preprocessing strategies, we consider that it is unnecessary to know the precise structure of the network. Given only general statistical properties of the network, we propose strategies that act on each node, depending only on locally accessible information, such as the degree of the node. We calculate the new percolation threshold $\tilde{\phi}_1^*$ of the modified network and the evolution of the giant connected component \tilde{S} . Above the threshold any two nodes will be able to establish an entangled state with probability \tilde{S}^2 , again, independently of the distance between them. Thus, quantum preprocessing can benefit communication in two ways: by lowering the percolation threshold and by an increase in the giant component size.

A. Network model

We consider a quantum network in which neighboring nodes share $n = 2$ copies of a bipartite pure entangled state of two qubits,

$$|\psi\rangle = \sqrt{\lambda_0}|00\rangle + \sqrt{\lambda_1}|11\rangle, \quad (8)$$

where $\sqrt{\lambda_0} \geq \sqrt{\lambda_1} \geq 0$ are its Schmidt coefficients. A partially entangled state can be converted into a maximally entangled state (*singlet* for short) with singlet conversion probability (SCP), which depends only on its largest Schmidt coefficient [32]. For the state $|\psi\rangle$, the SCP is

$$\phi_1 = \min[1, 2(1 - \lambda_0)]. \quad (9)$$

We consider edges that are of the form $|\psi\rangle^{\otimes 2}$ and, thus, can be converted to singlets with the SCP

$$\phi_2 = \min[1, 2(1 - \lambda_0^2)]. \quad (10)$$

With this probability two neighbors can establish a perfect channel between them. As discussed above, for two distant nodes this probability depends on the structure of the network that connects them.

B. Modifying the network: q -swap

In [13] we introduced a network transformation, the q -swap, that requires only local information of the network: the degree of a target node and the status of its neighbors. The q -swap is built on a basic transformation: entanglement swapping or swap [33]. In a subgraph with three nodes, the party at the target node c performs a Bell measurement on two qubits, each of them belonging to states $|\psi\rangle$ shared with different nodes, a and b (see Fig. 4). After this operation,

¹[www.keys.ch.pgp.net:11371/pks/]; public data available at [www.lysator.liu.se/~jc/wotsap/index.html].

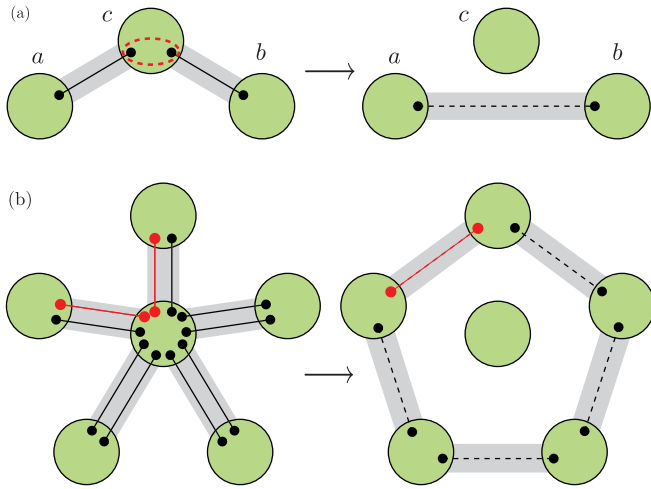


FIG. 4. (Color online) (a) Entanglement swapping and (b) q -swap (b). Small filled (black) circles represent qubits; large (green) circles, nodes; solid lines, states $|\psi\rangle$; and dashed lines, the resulting mixed state after entanglement swapping, with the same SCP as $|\psi\rangle$.

the central qubits become disentangled from a and b , but in return a mixed entangled state with the same SCP as $|\psi\rangle$ is created between a and b [5]. Note that this operation cannot be repeated with a fourth node because the newborn state shared between a and b is not of the form of $|\psi\rangle$. The q -swap performs swap transformations between successive pairs of neighbors of a central target node of degree q , thus changing an initial q -star with edges $|\psi\rangle^{\otimes 2}$ to a q -cycle with newborn edges, while the central target node becomes disconnected from the network (see Fig. 4). For a given network topology, we will see that performing q -swaps on nodes with certain degrees improves the threshold. It is worth noting, however, that in some instances the application of particular q -swaps may be counterproductive.

C. Percolation threshold and giant component

The main two figures of merit that we use to compare the two strategies are the percolation thresholds (ϕ_1^* and $\tilde{\phi}_1^*$ for the classic and q -swap strategies, respectively) and the size of the giant components (S and \tilde{S}). Since q -swaps disconnect vertices, which can be chosen not to be the two corresponding to the parties that want to communicate, the probability of connecting two remote nodes is in fact \hat{S}^2 , where $\hat{S} = \tilde{S}S_1/\tilde{S}_1$ and S_1 is the value of S at $\phi_1 = 1$. The percolation threshold tells us which is the minimum amount of entanglement needed for long-distance communication, while the square of the giant connected component size is the probability that any two nodes can communicate.

To compute these two values we use the generating function formalism described in Sec. II. The key probability distributions are those of finding a connected component of finite size s , either when a random vertex is chosen, P_s , or when a random edge is followed to one of its ends, R_s . A random edge is vacant with probability $R_0 = 1 - \phi_2$, giving a cluster of size 0. When it is occupied, then a node of degree

$k + 1$ is reached with probability r_k , giving access to k clusters. Therefore,

$$R_{s \geq 1} = \phi_2 \sum_{k=0}^{\infty} r_k \sum_{s_1, s_2, \dots, s_k} R_{s_1} R_{s_2} \dots R_{s_k} \delta_{s, 1 + \sum_{i=1}^k s_i}. \quad (11)$$

We have assumed that components are treelike, that is, that they do not have finite loops. This is indeed true for finite components, since an edge exiting such a component will reconnect back to itself with a probability proportional to $s/N \rightarrow 0$. The function generating R_s is then $h_R(x) = \sum_{s \geq 0} R_s x^s$, which gives the recurrence relation

$$h_R(x) = 1 - \phi_2 + \phi_2 x g_r[h_R(x)]. \quad (12)$$

It is crucial to note here that by restricting to finite s , we have explicitly excluded the infinite giant component from $h_R(x)$. Thanks to this, the previous treelike assumption holds.

We can proceed similarly with P_s . A random vertex has degree k with probability p_k , giving access to k clusters. The probability that this random vertex is in a component of size s is then

$$P_s = \sum_{k=1}^{\infty} p_k \sum_{s_1, s_2, \dots, s_k} R_{s_1} R_{s_2} \dots R_{s_k} \delta_{s, 1 + \sum_{i=1}^k s_i}. \quad (13)$$

Now the generating function for P_s is related to $h_R(x)$:

$$h_P(x) = x g_p[h_R(x)]. \quad (14)$$

Knowledge of $h_P(x)$ and $h_R(x)$ allows for the derivation of ϕ_1^* and S . The probability u that an edge connects to a finite component is the smallest real solution of $u \equiv h_R(1)$ in Eq. (12), which is, in general, a transcendental function. In fact, the percolation threshold is the value of ϕ_1 at which a solution $u < 1$ appears. Moreover, u^2 is the probability that the edge connects to a finite component through both ends, so with probability $1 - u^2$, a random edge belongs to the giant component (which is 0 below the threshold).

Similarly, the main quantity of interest, the giant component size, can be computed as the missing component in the whole network. The sum of all P_s , $h_P(1)$, gives the probability that a random vertex belongs to a finite component, while the probability S that it is in the giant component is $S = 1 - \sum_{s \geq 1} P_s = 1 - h_P(1)$. Again, this equation is usually transcendental and has to be solved numerically. For instance, the Erdős-Rényi model, with $g_p(x) = g_r(x) = e^{z(x-1)}$, has a giant component fraction $S = 1 - e^{-z\phi_2 S}$ [15]. In this case the solution can be expressed in terms of the Lambert W function,

$$S = 1 + \frac{1}{z\phi_2} W(-z\phi_2 e^{-z\phi_2}), \quad (15)$$

and the phase transition to $S > 0$ occurs at the well-known point $\phi_1^* = 1/z$. In contrast, first moments can usually be computed even when a closed expression for $h_P(x)$ and $h_R(x)$ is not known. As a relevant example, the average component size $\langle s \rangle = h'_P(1)$ is an important property of the network that provides an alternative way of finding the probability threshold: it is at this point that $\langle s \rangle$ diverges. From the

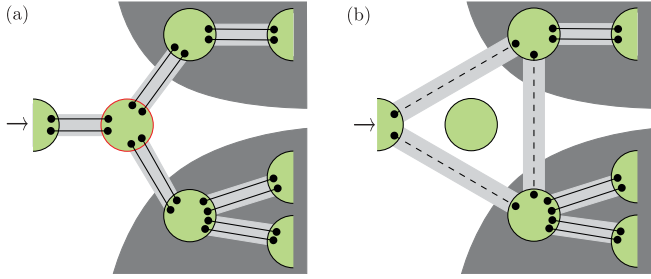


FIG. 5. (Color online) Example of the branching process before and after a 3-swap, starting at the leftmost node. (a) Before any operation the branching process arrives at a node of degree 3, leading to two components (in dark gray). (b) After the 3-swap, the branching process is already in a 3-cycle, each of its nodes belonging to one of the two components.

derivatives of Eqs. (12) and (14), it is immediate to find that this divergence can be traced back to that of

$$h'_R(1) = \frac{\phi_2}{1 - \phi_2 g'_r(1)}. \quad (16)$$

This brings the general result for the critical SCP $\phi_2^* = 1/g'_r(1)$ [34].

We now want to understand how the q -swap transformation changes the percolation properties of the network. Every particular q -swap can be implemented (or not) with probability Π_q (or $1 - \Pi_q$) on nodes of degree q . Giving the values for each Π_q specifies the quantum strategy. q -swaps introduce cycles, so components are no longer treelike and generating functions cannot be directly used. Note, however, that, since newborn edges cannot be reused, those cycles do not overlap between each other and can thus be treated as blocks of a treelike component by considering two steps in the branching process. We first compute the generating function for the probability R_s after q -swaps are done, $\tilde{h}_R(x)$. Now, instead of arriving at a vertex of degree q connecting to other $q - 1$ components, after a q -swap operation has been done we arrive at a cycle of q nodes (including the one we are coming from) connected via edges occupied with probability ϕ_1 (see Fig. 5). When edges are converted into singlets, the accessible nodes of this new q -cycle form a string of length l with probability

$$\begin{cases} \phi_1^q & \text{for } l = q, \\ q\phi_1^{q-1}(1 - \phi_1) & \text{for } l = q - 1, \\ (l + 1)\phi_1^l(1 - \phi_1)^2 & \text{for } l \leq q - 2. \end{cases}$$

For $l \leq q - 2$, l new components emerge, with the total size (including all the vertices in the cycle, except the starting one) probability generated by $\{x g_r[\tilde{h}_R(x)]\}^l$. For $l = q - 1$ and $l = q$, $q - 1$ components emerge, again with the total size probability generated by $\{x g_r[\tilde{h}_R(x)]\}^{q-1}$. The total size of this cycle and its emerging components is then generated by

$$C_q(x) = \sum_{l=0}^{q-2} (l + 1)\phi_1^l(1 - \phi_1)^2 \{x g_r[\tilde{h}_R(x)]\}^l + [q\phi_1^{q-1}(1 - \phi_1) + \phi_1^q] \{x g_r[\tilde{h}_R(x)]\}^{q-1}. \quad (17)$$

Therefore, the new $\tilde{h}_R(x)$ is of the same form as Eq. (12) plus a term $\tilde{h}_{R,q}(x)$ for each q -swap:

$$\tilde{h}_R(x) = 1 - \phi_2 + \phi_2 x g_r(\tilde{h}_R(x)) + \sum_{q \geq 2} \Pi_q \tilde{h}_{R,q}(x), \quad (18)$$

$$\tilde{h}_{R,q}(x) = r_{q-1} \{(\phi_2 - 1) - \phi_2 x [\tilde{h}_R(x)]^{q-1} + C_q(x)\}.$$

At this stage we can already calculate $\tilde{\phi}_1^*$ as the smallest value of ϕ_1 for which there exists a positive solution $\tilde{u} = \tilde{h}_R(1) < 1$ to (18) at $x = 1$. It is easy to convince oneself that each separate contribution $\tilde{h}_{R,q}(1)$ either increases or lowers the percolation threshold, and therefore for the optimal strategy each Π_q is either 0 or 1.

For the new $\tilde{h}_P(x)$ we need to consider that not all nodes of degree q are suitable targets of q -swaps, since they cannot be performed on adjacent nodes. Therefore, given a node of degree q there is a probability η_q that a q -swap can be performed on it. If the q -swap is performed on a node, then it changes its degree from q to 0, and hence

$$\tilde{h}_P(x) = x g_p[\tilde{h}_R(x)] + x \sum_{q \geq 2} \Pi_q \eta_q p_q \{1 - [\tilde{h}_R(x)]^q\}. \quad (19)$$

By using the solution $\tilde{u} = \tilde{h}_R(1)$ here, we can obtain the size of the giant connected component, $\tilde{S} = 1 - \tilde{h}_P(1)$. This gives the probability \tilde{S}^2 that two distant nodes are connected by a path of singlets.

The probability η_q depends on which degrees are targets of q -swaps and on how the network is traversed to operate on the nodes. To compute its value we need to consider maximal clusters consisting of nodes where all vertices are of any target degree q —the border of such clusters is necessarily made of nodes of degree different from q , and hence operations can be done independently on every cluster. As an example, let us discuss the simplest case of only performing 2-swaps. Starting from a random vertex of degree 2, we find a cluster of vertices of same degree 2 whose size is s with probability $s(1 - r_1)^2 r_1^{s-1}$. By acting on a node, and then on every second node, there are two possible values for the number of operations done in each cluster, $\lceil s/2 \rceil$ and $\lfloor s/2 \rfloor$ (Fig. 6), which coincide for s even. This gives a maximum and minimum value for η_2 :

$$\eta_2^{(\max)} = \sum_{s \geq 1} s(1 - r_1)^2 r_1^{s-1} \frac{\lceil s/2 \rceil}{s} = \frac{1}{1 + r_1}, \quad (20)$$

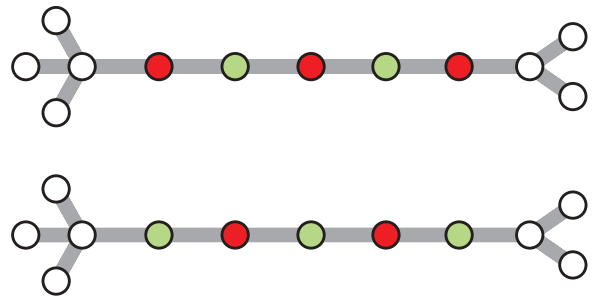


FIG. 6. (Color online) Two clusters of five nodes with degree 2. Nodes are large circles: white if their degree is different from 2, dark gray (red) if they are operated on, and light gray (green) if they are not. Top: Operations are done at nodes 1, 3, and 5, leading to $\eta_2^{(\max)}$. Bottom: Operations are done at nodes 2 and 4, leading to $\eta_2^{(\min)}$.

$$\begin{aligned}\eta_2^{(\min)} &= (1 - r_1)^2 + \sum_{s \geq 2} s(1 - r_1)^2 r_1^{s-1} \frac{\lfloor s/2 \rfloor}{s} \\ &= \frac{1 - (1 - r_1)r_1^2}{1 + r_1}.\end{aligned}\quad (21)$$

Note that for clusters of size $s = 1$, an operation is always done. When operations are performed starting from a random vertex in each cluster of vertices with degree 2, one needs to take into account the number of vertices s and t at odd and even (including 0) distance from the first vertex: operations will be performed on a fraction $t/(t + s)$ of the cluster. The probability $\xi(s, t)$ of starting in a vertex of degree 2 such that it has s neighbors of degree 2 at odd distance and t at even distance is

$$\xi(s, t) = \binom{2}{1 + s - t} (1 - r_1)^2 r_1^{s+t-1} t \quad (22)$$

if $|s - t| \leq 1$ and 0 otherwise. For general q , this probability can be found by generating functions similar to the ones described before; see the Appendix for more details. Given the probability $\xi(s, t)$, then the value for η_2 when operations are started at each cluster of target vertices is

$$\eta_2^{(\text{rand})} = \sum_{s, t} \frac{t}{t + s} \xi(s, t) = \frac{r_1 + (1 - r_1)^2 \operatorname{atanh}(r_1)}{2r_1}. \quad (23)$$

Figure 7 show $\eta_2^{(\max)}$, $\eta_2^{(\min)}$, and $\eta_2^{(\text{rand})}$ together with numerical simulations performing 2-swaps by traversing the graph with a breadth first search (BFS), as described in the following section. The numerical values for η_2 are close to the maximum value because it is much more likely that the traversal of graph started outside most of the degree 2 clusters (e.g., arriving through one of the white nodes in Fig. 6), thus performing the maximum number of operations in them.

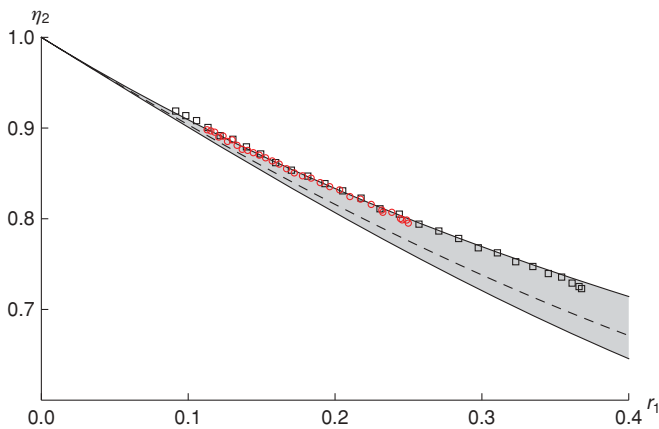


FIG. 7. (Color online) Probability η_2 of performing a 2-swap, given a vertex of degree 2. Upper and lower lines correspond to Eqs. (20) and (21), respectively; squares, to Erdős-Rényi network simulations; and circles, to scale-free network simulations. All simulations were performed with $N = 10^6$ and breadth first search traversal of the graph.

D. Network examples and simulations

Here we present some examples of entanglement percolation in the networks described in Sec. III, and we provide analytic solutions for paradigmatic cases. To check these results and extend them to correlated and real-world networks, we have performed computer simulations with various network models. Graphs with uncorrelated degree distribution are relatively easy to generate [15]. First, a set of N numbers $\{k_i\}$ randomly chosen to follow the desired degree distribution is generated, so each vertex i has k_i stubs or “half-edges” associated with it. If the sum $\sum_i k_i$ is odd, a new set is generated until an even sum is obtained, so all stubs can be joined. Then pairs of stubs are selected randomly and joined to form edges until there are no stubs left. In our simulations we did not allow self-loops or multiple edges. The quantum preprocessing is done by traversing all the graph with a BFS, which starts at a random root vertex and explores all the neighboring nodes at distance 1, 2, . . . , until all the vertices in the component have been visited. After that, another BFS is done starting from a random unexplored vertex in another component, until all components have been examined. At each discovered vertex, the local structure is changed from a q -star to a q -cycle if the vertex degree is one of the target degrees and if none of the edges in the star have already been used.

For the Bethe lattice with coordination number q , $g_p(x) = x^q$ and $g_r(x) = x^{q-1}$. In this network the phase transition occurs at $\phi_2 = (q - 1)^{-1}$ and

$$(q - 1)^{-1} = (1 - \phi_1)^{-1} \{2\phi_1 + \phi_1^q [\phi_1(q - 1) - (q + 1)]\}$$

after q -swap is applied. Therefore, q -swap always gives a better threshold except for the special case $q = 2$ of an infinite one-dimensional chain, where the probability decays exponentially with the distance.

In the Erdős-Rényi network, before any transformation the threshold is given by $\phi_2 = 1/z$. After, for example, the 2-swap and 3-swap operations, the thresholds are, respectively,

$$\frac{1}{z} = \phi_2 + e^{-z} [-\phi_2 + z(2\phi_1 - \phi_1^2)] \quad (24)$$

and

$$\frac{1}{z} = \phi_2 + ze^{-z} [-\phi_2 + z(1 + \phi_1 - \phi_1^2)]. \quad (25)$$

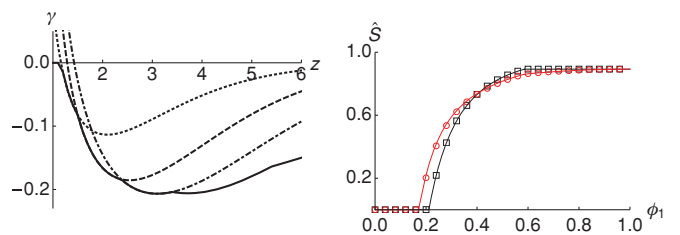


FIG. 8. (Color online) Erdős-Rényi network. (a) Gain γ as a function of the mean degree z after 2-swap (dotted line), 2,3-swap (dashed line), 2,3,4-swap (dot-dashed line), and optimal q -swaps (solid line). (b) Normalized size \hat{S} of the the giant connected component (GCC) as a function of ϕ_1 for $z = 2.5$, before (squares) and after (circles) 2,3-swap; $N = 10^6$.

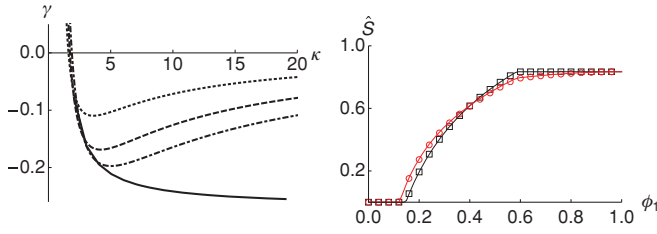


FIG. 9. (Color online) Scale-free network, $\tau = 1$. (a) Gain γ as a function of the cutoff k after 2-swap (dotted line), 2,3-swap (dashed line), 2,3,4-swap (dot-dashed line), and optimal q -swaps (solid line). (b) Normalized size \hat{S} of the GCC as a function of ϕ_1 for $\kappa = 4$, before (squares) and after (circles) 2,3-swap; $N = 10^6$.

Figure 8 shows the evolution of the giant connected component before and after the transformations, with perfect agreement between analytical and numerical results. Figure 8 also shows the gain $\gamma = (\tilde{\phi}_1^* - \phi_1^*)/\phi_1^*$ in the percolation threshold, which in some situations is higher than 20%. The performance of different q -swaps depends on the mean degree z , usually improving the threshold for those operations which act on nodes whose degree is around z . Figure 9 shows similar results for the giant connected component evolution and the gain in scale-free networks with $\tau = 1$. In this case the gain can be about 25%.

For the Watts-Strogatz model, which is correlated, and the World Wide Web network, the above approach is not valid because the treelike assumption does not hold. However, numerical simulations show that q -swaps can also provide an improvement in the percolation threshold, $\tilde{\phi}_1^* < \phi_1^*$. Figure 10 shows the threshold probability for the Watts-Strogatz before and after 2-swap and the size of the giant connected component. Figure 11 shows the size of the giant connected component for the World Wide Web.

Note that, in general, it may be counterproductive to perform q -swaps. In Figs. 10 and 11 we see that for some values of ϕ_1 the giant connected component fraction S without preprocessing is larger than \hat{S} . This often happens around $\phi_1 = 2 - \sqrt{2}$. This is precisely the point where the edges in the unmodified network can be directly converted into singlets with $\phi_2 = 1$, that is, all connections become ideal channels and S attains its maximal value $S = S_1$. Obviously at this stage any preprocessing cannot further increase the size of the connected component, and it will most likely decrease it.

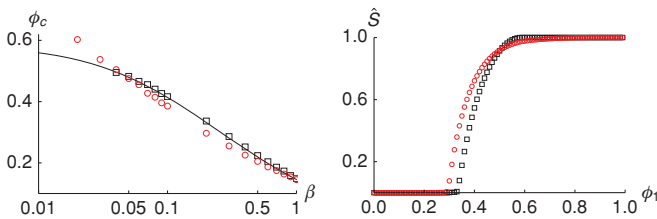


FIG. 10. (Color online) Watts-Strogatz network. (a) Percolation threshold ϕ_1^* as a function of shortcut probability β before (squares) and after (circles) 2-swap. The solid line is the analytic result from Ref. [14]. (b) Normalized size \hat{S} of the GCC as a function of ϕ_1 for $\beta = 0.2$, before (squares) and after (circles) 2-swap; $N = 10^6$.

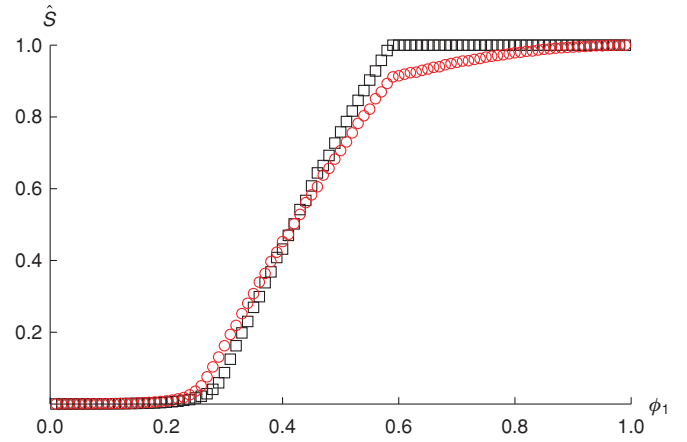


FIG. 11. (Color online) World Wide Web network [31], with a cutoff at $k = 15$, before (squares) and after (circles) 2,3-swap.

V. MIXED-STATE NETWORKS

A network with nodes connected by pure states is an abstraction that gives insight into the possibilities of long-distance entanglement in complex networks, enabling perfect teleportation between distant parties when at least a path of maximally entangled states is created. In general, however, states connecting two neighbors are noisy and need to be described by mixed states. In this situation, the optimal fidelity of teleportation f is directly related to the maximal singlet fraction F [35] by

$$f = \frac{Fd + 1}{d + 1}, \quad (26)$$

where d is the dimension of each part of the bipartite state and F is defined as the maximal overlap of a state ρ with a maximally entangled state $|\Psi\rangle = \frac{1}{\sqrt{d}} \sum_i |ii\rangle$:

$$F(\rho) = \max_{|\Psi\rangle} \langle \Psi | \rho | \Psi \rangle. \quad (27)$$

Entanglement percolation in the mixed-state scenario has already been addressed in regular lattices with connections consisting of singlets that have suffered an amplitude damping [9,10]. There, a hybrid swapping strategy is proposed for this type of connections, which could also be used to build a mixed-state q -swap to act on complex networks with at least four states per edge. In another approach, Perseguers gives a fidelity threshold for the links above which long-distance quantum communication in the presence of noise is possible for an infinite cubic lattice [8].

Communication in noisy networks can be considered from another perspective. The noise in the connections fixes a limit l in the maximum number of nodes through which the information can be repeated before it becomes too corrupted [3]. In this limited-path-length scenario, the total number of vertices that a given node can communicate to also depends strongly on the structure of the communication network (Fig. 12). This is related to the average path length l_{av} : the length of the shortest path averaged over all possible pairs of nodes. All nodes within this distance constitute a significant fraction of the network. Therefore, for a path-length limit l above the average l_{av} , communication will be possible among

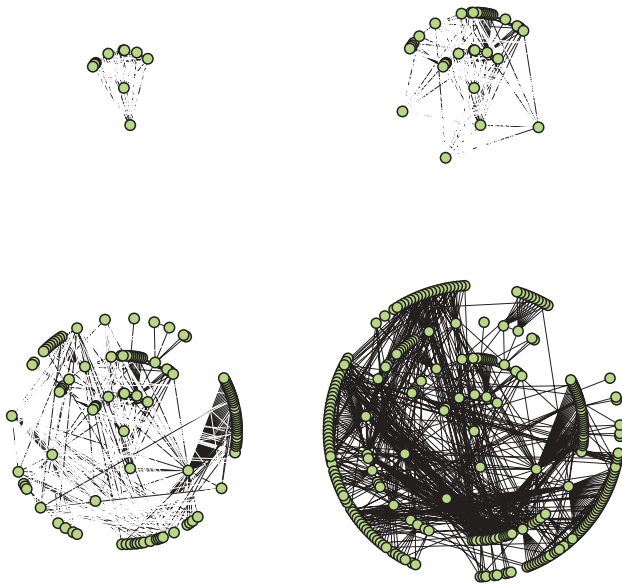


FIG. 12. (Color online) For a limited path length, cluster growth depends on the network topology. Here, clusters of limited path length $l = 1, 2, 3$, and 4 in the OpenPGP Web of Trust, with sizes of 11, 37, 115, and 286.

an important number of nodes. Since the limiting l is finite, the giant connected component appears only in models where l_{av} is also finite. In general, this only happens if the network size is finite too. The question, then, is whether a small l will suffice to cover a significant fraction of the network. In finite d -dimensional networks, the average path length scales as $l_{av} \sim N^{1/d}$. However, the average path length of many complex networks scales *logarithmically* with the size of the network. This property is known as the small-world effect and appears also in many real-world communication networks such as the Internet. In this case, to access a significant fraction of nodes, only a small number of edges need to be traversed. Small-world models are therefore the first candidates where losses by noise can be balanced by a short path length.

The problem of *limited-path percolation* was also addressed in a different approach by López *et al.* [36]. In their model, they calculate the percolation phase transition under the assumption that communication is only effective if the new minimum path length between two nodes does not exceed a multiple of the original path length between them. Thus, in their study the limitation in the path length comes from the topology of the network and not from the nature of channels connecting nodes, which fixes a constant limit of nodes through which the information can be repeated.

Here, we are interested in the number of nodes that can exchange quantum information with a given node for some fixed minimum fidelity or, similarly, with what probability two random nodes can reliably communicate between them. We consider a scenario similar to that in the previous sections, but replacing pure-state connections with generic entangled mixed states. Here, no quantum preprocessing is possible. However, we will find that the complex network structure (in particular, the small-world effect) allows us to

interconnect a large number of nodes using the standard entanglement percolation strategy. We start by doing some numerical simulations and then derive the generating functions for limited-path percolation and compute the limited average size in noncorrelated networks and the Watts-Strogatz model.

A. Network simulations

We begin by simulating different models of networks. For simplicity we consider that edges hold a single copy of a two-qubit state ρ_F with maximum singlet fidelity $F > 1/2$, so that the classical limit of $f = 2/3$ in the teleportation fidelity can be exceeded. Note that, as long as ρ_F is entangled, this limit can be achieved even if $F < 1/2$ by locally increasing the singlet fidelity through trace-preserving local operations and classical communication (LOCC) [37]. By applying random bilateral rotations, ρ_F can be brought into a Werner state,

$$\rho_F = F|\Psi^-\rangle\langle\Psi^-| + \frac{1-F}{3}|\Psi^+\rangle\langle\Psi^+| + \frac{1-F}{3}|\Phi^-\rangle\langle\Phi^-| + \frac{1-F}{3}|\Phi^+\rangle\langle\Phi^+|, \quad (28)$$

which has the same singlet fidelity F . This state can also be written as

$$\rho_\alpha = \alpha|\Psi^-\rangle\langle\Psi^-| + (1-\alpha)\frac{\mathbb{1}}{4}, \quad (29)$$

with $\alpha = (4F - 1)/3$. It can be interpreted as the result of transmitting a pure singlet through a depolarizing channel. Hence, when a state is teleported through l of such edges [2,3,38], its fidelity is 1 with probability α^l and $1/2$ otherwise, so its final fidelity is $f_l = (1 + \alpha^l)/2$. This fidelity decreases exponentially with the distance l and makes such a communication scheme useless in networks such as linear chains or regular lattices, where the typical distance between two nodes scales as the size of the network. However, as we have discussed, the typical distance in many complex networks scales only logarithmically. The maximum distance l that information can travel is fixed by the minimum fidelity f_{min} required at the end point and by the purity α of the channels:

$$l = \left\lfloor \frac{\ln(2f_{min} - 1)}{\ln \alpha} \right\rfloor. \quad (30)$$

This means that, even if there exists a path between a sender and a receiver in a network, it will only be useful if the length of this path is below a certain threshold.

We performed extensive simulations of networks where neighboring nodes share a state, (29), and considered the classical limit as the minimum required fidelity, $f_{min} = 2/3$. For small networks ($N \lesssim 10^4$) we performed the calculations over several network realizations and then averaged the results. For bigger networks, a single network realization is usually enough due to the self-averaging. The l -limited average cluster size $\langle s_l \rangle$ is an especially relevant parameter, which amounts to the probability that two nodes can communicate with fidelity $f > f_{min}$.

We have thus calculated $\langle s_l \rangle$ for different network models and sizes. In Fig. 13 we plot the normalized size $\langle s_l \rangle / N$ as a function of $l - l_{av}$ for the Erdős-Rényi model, with average path length $l_{av} \sim \ln N / \ln z$ [39]. For different network sizes the curves collapse, supporting a linear N dependence

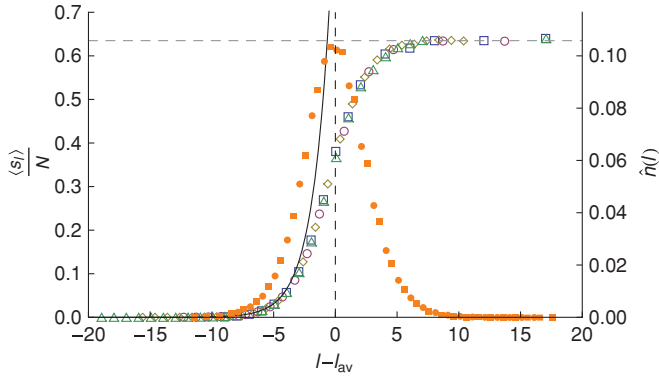


FIG. 13. (Color online) Normalized l -limited average component size $\langle s_l \rangle / N$ as a function of $l - l_{av}$ for the Erdős-Rényi network with $k = 2$ and network sizes $N = 10^3, 10^4, 10^5$, and 10^6 (squares, circles, diamonds, and triangles). Superimposed filled (orange) symbols show the shape of the path-length distribution normalized by the total number of possible vertex pairs, $\hat{n}(l) = 2n(l)/N(N - 1)$. Solid (black) line is Eq. (34); horizontal dashed line is the square of the GCC at $\phi_1 = 1$ [see Eq. (15)].

$\langle s_l \rangle \sim N$ for fixed l . Similar results have recently been found for the average number of nodes at an exact distance l from a random central node [40]. Regarding the dependence in l , our results show that the average size grows exponentially with l for $l \ll l_{av}$ but deviate from this behavior when l is close to the average path length, saturating to the maximum component size shortly after l_{av} . This deviation is due to the depletion of nodes at distance $l > l_{av}$. In Fig. 13 we also plot the path-length distribution, that is, the number of pairs $n(l)$ separated by a distance l , normalized by the total number of pairs $N(N - 1)/2$. Again, both curves, $N = 10^3$ and $N = 10^4$, collapse, thus supporting a dependence $n(l) \sim N^2$. We also found similar results for the scale-free and the Watts-Strogatz models. It is interesting to note that, while l_{av} grows with the size of the network, the width of the path-length distribution remains constant. Thus, for large networks a small increase in α near l_{av} leads to an abrupt change in $\langle s_l \rangle / N$. This is in stark

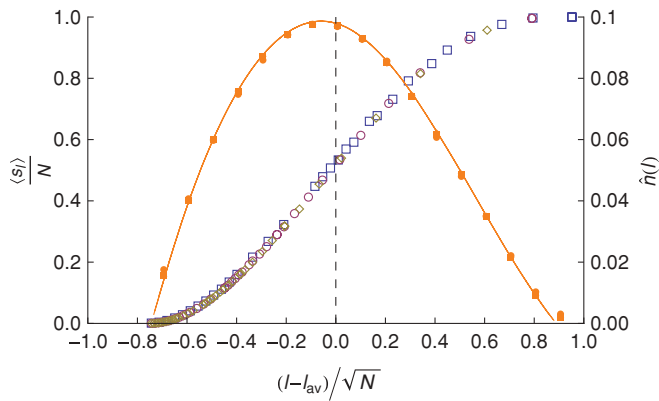


FIG. 14. (Color online) Normalized l -limited average component size $\langle s_l \rangle / N$ as a function of $(l - l_{av})N^{-1/2}$ for the honeycomb two-dimensional network with network sizes $N = 1014, 5046$, and 10086 (squares, circles, and diamonds, respectively). Superimposed filled (orange) symbols show the normalized histogram of the path-length distribution.

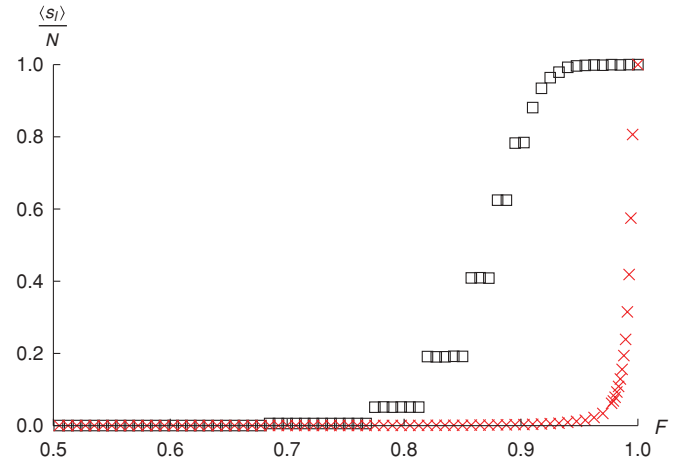


FIG. 15. Normalized l -limited average component size $\langle s_l \rangle / N$ as a function of singlet fidelity F in the biggest component OpenPGP Web of Trust (squares) and a honeycomb two-dimensional lattice (crosses); $N \sim 3 \times 10^4$.

contrast to regular lattices, where both the mean and the width scale as $N^{1/d}$. For instance, in Fig. 14 we plot $\langle s_l \rangle / N$ and the path-length distribution of the honeycomb two-dimensional lattice as a function of $(l - l_{av})N^{-1/2}$. The collapse of the curves confirms the $N^{1/d}$ length-scale dependence.

As an example of a real-world network, we considered the OpenPGP Web of Trust. Figure 15 shows the probability that two arbitrary nodes can communicate with fidelity $f > 2/3$ as a function of the singlet fraction F . Again, the comparison with a Honeycomb lattice of the same size shows that the small-world property of the complex networks allows for faithful communication between most of the nodes in the network for reasonable values of the noise, while in regular lattices this is only possible for nearly pure states.

B. Average component size in limited-path percolation

We now proceed to derive the generating functions for the limited-path-percolation problem. In this case, we are interested in the distribution of sizes s of the components that can be reached by only l steps through edges that are always occupied. As in the nonlimited case, there are two different distributions, $P_s^{(l)}$ and $R_s^{(l)}$, for the cases where a random vertex or a random edge is selected. The two corresponding generating functions, $h_P^{(l)}$ and $h_R^{(l)}$, read as

$$h_P^{(l)}(x) = \begin{cases} x & \text{for } l = 0, \\ x g_p [h_R^{(l-1)}(x)] & \text{for } l \geq 1, \end{cases} \quad (31)$$

and

$$h_R^{(l)}(x) = \begin{cases} x & \text{for } l = 0, \\ x g_r [h_R^{(l-1)}(x)] & \text{for } l \geq 1. \end{cases} \quad (32)$$

Note that all edges are occupied with probability 1. The generalization to a different occupancy probability is straightforward, but not needed here.

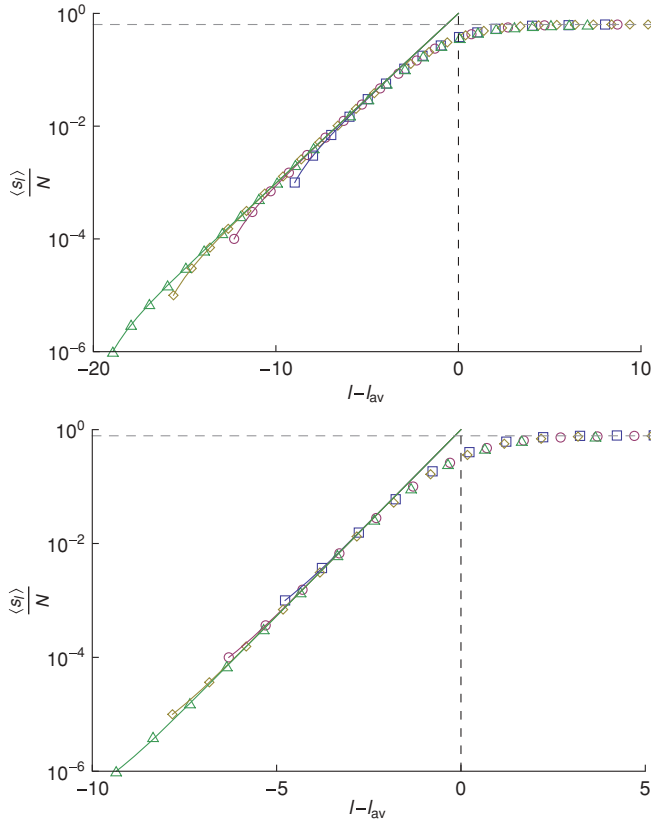


FIG. 16. (Color online) Normalized l -limited average component size $\langle s_l \rangle / N$ as a function of $l - l_{av}$ for (a) the Erdős-Rényi network and (b) the scale-free network. Points are simulation results for network sizes $N = 10^3, 10^4, 10^5$, and 10^6 (squares, circles, diamonds, and triangles, respectively). Solid lines correspond to Eq. (34); horizontal dashed lines are the values of S_1^2 .

As before, we are now ready to obtain the l -limited average size,

$$\langle s_l \rangle = \left. \frac{dh_p^{(l)}(x)}{dx} \right|_{x=1} = 1 + g_p'(1)h_R^{(l-1)}(1). \quad (33)$$

By solving the recurrence equation given by $h_R^{(l)}(1)$ with the boundary condition $h_R^{(0)}(1) = 1$, we find

$$\langle s_l \rangle = \begin{cases} 1 & \text{for } l = 0, \\ 1 + g_p'(1) \frac{1 - (g_r'(1))^l}{1 - g_r'(1)} & \text{for } l \geq 1. \end{cases} \quad (34)$$

This equals to the probability that any two nodes will be able to communicate with fidelity above f_{\min} . Figure 16 shows this result for the Erdős-Rényi and the scale-free model, with very good agreement between theoretical and numerical results below l_{av} .

As discussed above, this exponential growth of $\langle s_l \rangle$ is valid for l well below l_{av} . Our numerical simulations show that the validity of this approximation can be extended to values near l_{av} . Figure 13 shows that the path-length distribution is very peaked around l_{av} , and its width is independent of N . This implies, on one hand that our analytical approach holds true for values of l that fall out of this finite width (approaching from below); see Fig. 16. In contrast, the finite width implies

that if l is a few steps beyond l_{av} , then most of the nodes in the components will be reached before the limit distance is attained. In this situation, Eqs. (31) and (32) approach the nonlimited case of (14) and (12) with $\phi_1 = 1$, and the size of the giant component S_l tends to the nonlimited size S_1 . Therefore, for networks with the small-world property, that is, $l_{av} \sim \log N$, one can interconnect with a threshold fidelity (say, the classical benchmark $f = 2/3$) any arbitrary pair of nodes in the network, provided that the singlet fraction of the edges scales as $F = 1 - O(1/\log N)$ with the size of the network, which is clearly less stringent than the analogous constrain for d -dimensional networks $F = 1 - O(N^{-1/d})$.

We also consider the Watts-Strogatz model presented in Sec. III, which has a base circular lattice of size N with βN randomly added shortcuts. In this case the derivation of the probability that a random vertex belongs to an l -limited cluster of size s , $P_s^{(l)}$, and its generating function $h_p^{(l)}(x)$ uses the formalism of “local clusters” introduced in [14]. These local clusters are clusters in the base lattice (without considering the shortcuts). For a given l , the local cluster is always of size $2l + 1$. Thus, a shortcut at distance $\lambda - 1$ from the starting vertex leads to a (global) cluster of size s' with probability $P_{s'}^{(l-\lambda)}$. A random shortcut emerges from the starting vertex with probability $1/N$, from a vertex at distance λ with probability $2/N$, and lies outside the local cluster with probability $(N - 2l + 1)/N$. Hence, that shortcut will lead to a cluster of size s with a probability given by the generating function:

$$f(x) = 1 - \frac{1}{N} \left[2l - 1 - h_p^{(l-1)}(x) - 2 \sum_{\lambda=2}^l h_p^{(l-\lambda)}(x) \right].$$

There are $2\beta N$ shortcut end points that can similarly contribute to the total size of the cluster. Recalling that the generating function of the sum of sizes is the product of the generating function of each size, we find

$$h_p^{(l)}(x) = x^{l+1} f(x)^{2\beta N}, \quad (35)$$

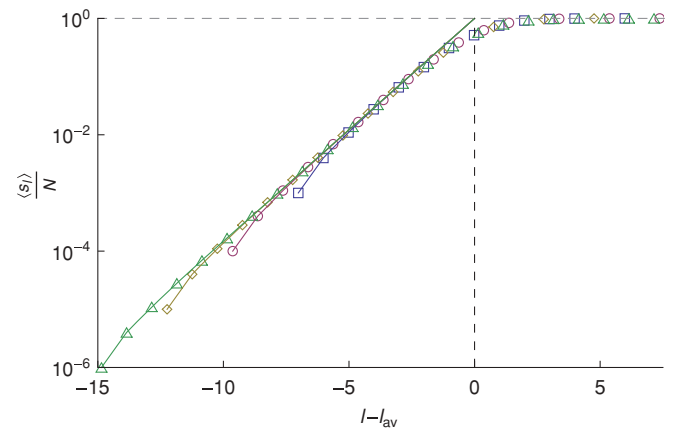


FIG. 17. (Color online) Normalized l -limited average component size $\langle s_l \rangle / N$ as a function of $l - l_{av}$ for the Watts-Strogatz network. Points are simulation results for network sizes $N = 10^3, 10^4, 10^5$, and 10^6 (squares, circles, diamonds, and triangles, respectively); lines correspond to the solution of Eq. (37).

where $x^{(l+1)}$ is the generating function corresponding to the starting “local” cluster. In the limit of large N this can be simplified to

$$h_p^{(l)}(x) = x^{1+2l} e^{-2\beta} \left[2l - 1 - h_p^{(l-1)}(x) - 2 \sum_{\lambda=2}^l h_p^{(l-\lambda)}(x) \right]. \quad (36)$$

Again, we can obtain the limited average size by taking the first derivative at $x = 1$. For $l = 0$, $\langle s_0 \rangle = 1$. For $l \geq 1$, this results in the recurrence equation

$$\begin{aligned} \langle s_l \rangle &= 1 + 2l + 2\beta \left[\langle s_{l-1} \rangle + 2 \sum_{\lambda=0}^{l-2} \langle s_\lambda \rangle \right] \\ &= \langle s_{l-1} \rangle + 2 + 2\beta (\langle s_{l-1} \rangle + \langle s_{l-2} \rangle), \end{aligned} \quad (37)$$

which can be exactly solved. Figure 17 shows this result. We want to stress the fact that from these generating functions, (31) and (36), one can also calculate the probability $P_s^{(l)}$ up to any s by solving $s + 1$ iterations of them and using Eq. (4).

VI. CONCLUSIONS

We have demonstrated that quantum complex networks offer a powerful framework for entanglement distribution in large systems. Regardless of their intricate structure, complex networks can be studied by their statistical properties, which allows us to analytically compute some interesting properties and to deal with them without knowing their exact structure. Here we have considered entanglement percolation in networks where connections are built on pure, nonmaximal bipartite entangled states and have studied a local quantum preprocessing of the network that can significantly decrease the percolation threshold and therefore allow quantum communication for a lower level of entanglement. The quantum preprocessing we have proposed is local in two senses. First, quantum operations are always done on qubits that belong to the same node. Second, the decision whether or not to perform this operation depends on the local structure of the network (the degree of the target node and the status of its neighbors) and on information about general statistical properties of the network. We have calculated the percolation threshold, which marks the minimum level of entanglement needed to entangle two distant nodes with finite probability. We have also computed this probability, which amounts to the square of the giant connected component in the network. These results are analytical for networks with uncorrelated degree distribution and can be compared to previous results in classical networks, which shows that the preprocessing can substantially improve communication over such networks by manipulating its local structure. We have also studied numerically the Watts-Strogatz small-world model and a real-world network, and have found a similar behavior.

In this approach, the links between nodes are pure quantum states. A more realistic scenario, however, needs to consider noise in the connections. Here we have thus considered the situation in which such connections are made of noisy mixed states.

We have shown that in complex networks a direct implementation of the entanglement percolation strategy, without quantum preprocessing, allows for faithful quantum communication (above a fixed fidelity threshold) between a large

number of nodes. The noise severely limits the number of steps or connections through which information is transmitted. However, in complex networks, one can reach a sizable amount of nodes with a moderately low number of steps. If the fidelity threshold allows for a path length slightly higher than the average path length, all nodes in the giant component become faithfully connected. The path-length distribution is peaked at low values (scaling as $\log N$ in complex networks versus $N^{1/d}$ in d -dimensional lattices) and has finite width (constant in N versus $N^{1/d}$). This implies that in complex networks a finite fraction of faithfully connected nodes appears for much smaller limiting path lengths and reaches the giant component size abruptly. Hence, here the advantage of complex networks is twofold: the average path length which marks the transition scales logarithmically with the network size, and the additional steps needed to reach the nonlimited scenario is finite.

We have shown that new phenomena appear if networks and the operations one can performed on them are governed by the laws of quantum mechanics. This has been known for regular lattices, but the rich properties of complex networks still remain widely unexplored in the quantum setting. Our results on percolation, together with new behavior found in the emergence of subgraphs in quantum random networks [41], are examples of these phenomena.

Our results also contribute to the field of classical complex network. We have given analytical results for the gain in the percolation thresholds and the size of the giant component for uncorrelated complex networks that undergo a set of local inversions (transformation that produce the complement of the induced subgraph of the target node). The problem at hand of studying how critical properties of a network can be drastically modified by a given set of network transformations might be of general interest to other disciplines in the field. Finally, we have addressed the problem of limited-path percolation in uncorrelated and small-world complex networks.

ACKNOWLEDGMENTS

We acknowledge financial support from the Spanish ME through FPU Grant No. AP2008-03048 (M.C.); from MICINN through the Ramón y Cajal program (J.C.) and Projects No. FIS2008-01236 and QOIT (CONSOLIDER2006-00019); and from the Generalitat de Catalunya CIRIT, under Contract No. 2009SGR985.

APPENDIX: CALCULATION OF η_q

As we said, the probability η_q depends on the target degrees $\{q_i\}$ and on how the network is traversed. By $\eta_q^{(\text{rand})}$ we denote the probability η_q when a q -swap is first done in a random vertex with target degree, and then the cluster of vertices with degree belonging to $\{q_i\}$ is traversed by a BFS, performing q -swaps whenever possible (i.e., at every second step). After that, another vertex with a target degree which has not yet been explored is selected, and its cluster traversed, until all target vertices have been checked. Such clusters consist of vertices of degree $k \in \{q_i\}$ that are connected by at least one path whose vertices also have a degree in $\{q_i\}$ and to which no more vertices of degree k can be added. Figure 18 shows an example of three of such clusters when the target degrees are 2

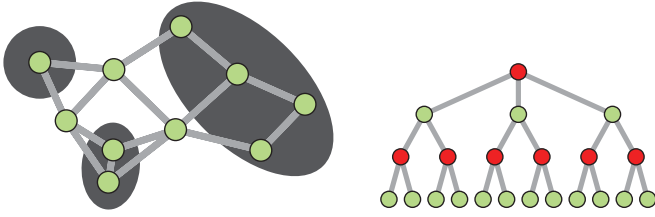


FIG. 18. (Color online) Left: Example of a connected component with three clusters (dark gray) of degrees 2 and 3. Right: Branching process in $\eta_3^{(\text{rand})}$; 3-swaps are made on dark-gray (red) nodes, which are the t nodes at an even distance from the top one.

and 3. A random vertex of degree $k \in \{q_i\}$ belongs to a cluster with t vertices at an even distance (including itself) and s at an odd distance with probability $\xi(s, t)$. In this cluster of size $s + t$, t q -swaps are made. The probability $\eta_q^{(\text{rand})}$ is then

$$\eta_q^{(\text{rand})} = \sum_{s,t} \frac{t}{s+t} \xi(s, t).$$

The function generating $\xi(s, t)$ can be computed similar to Eqs. (12) and (14). In this case, it is a function of two variables: $h_\xi(x, y) = \sum_{s,t \geq 0} \xi(s, t) y^s x^t$. Two more distributions are needed: $S(s, t)$ and $T(s, t)$ are the probabilities of arriving at a vertex of the given degree (or degrees) which is at an odd or even distance from the starting vertex, respectively, and which belongs to a cluster of s extra vertices at an odd distance and t at an even distance. The corresponding generating functions depend on each other:

$$h_S(x, y) = 1 - \sum_q \Pi_q r_q + y \sum_q \Pi_q r_q [h_T(x, y)]^{q-1}, \quad (\text{A1})$$

$$h_T(x, y) = 1 - \sum_q \Pi_q r_q + x \sum_q \Pi_q r_q [h_S(x, y)]^{q-1}, \quad (\text{A2})$$

and the function generating $\xi(s, t)$ is

$$h_\xi(x, y) = x \sum_q \Pi_q [h_S(x, y)]^q. \quad (\text{A3})$$

This allows computation of $\xi(s, t)$ by taking partial derivatives in x and y . As in the case of Eqs. (14) and (19), $h_\xi(x, y)$ is in

general a transcendental function and has to be solved numerically. However, in some cases it can be solved analytically. In the case of 2-swap only ($\Pi_2 = 1$, $\Pi_{q \neq 2} = 0$), Eq. (A3) simplifies to the closed form

$$h_\xi(x, y) = \frac{x(1-r_1)^2(1+r_1y)^2}{(1-r_1^2xy)^2}. \quad (\text{A4})$$

The probability $\xi(s, t)$ in Eq. (22) is then

$$\begin{aligned} \xi(s, t) &= \frac{1}{s!t!} \left. \frac{\partial^s \partial^t h_\xi(x, y)}{\partial y^s \partial x^t} \right|_{x,y=0} \\ &= \binom{2}{1+s-t} (1-r_1)^2 r_1^{s+t-1} t \end{aligned} \quad (\text{A5})$$

if $|s-t| \leq 1$ and 0 otherwise.

Alternatively, for the case of a single target degree, $\eta_q^{(\text{rand})}$ can also be computed exactly up to the n th order in r_{q-1} by the branching process depicted in Fig. 18. The process begins at step 0, with $k_0 = 1$ vertices of degree q . At step 1, k_1 vertices out of $qk_0 = q$ are of degree q with binomial probability

$$\binom{q}{k_1} r_{q-1}^{k_1} (1-r_{q-1})^{q-k_1}.$$

At following steps $i \geq 2$ in the branching process, there are $(q-1)$ new vertices for each previous vertex of degree q . Thus, in every step, k_i vertices are of degree q with probability

$$\binom{(q-1)k_{i-1}}{k_i} r_{q-1}^{k_i} (1-r_{q-1})^{(q-1)k_{i-1}-k_i}.$$

Operations are made on vertices at even steps. Note that every new step in the branching process involves higher orders in r_{q-1} . Therefore, the expansion of η_q up to order n is obtained by summing the contributions of the first n steps:

$$\begin{aligned} \eta_q^{(\text{rand})} &= \sum_{\{k_i\}} \frac{\sum_{i=0}^{\lfloor n/2 \rfloor} k_{2i}}{\sum_{i=0}^n k_i} \binom{q}{k_1} \prod_{i=2}^n \binom{(q-1)k_{i-1}}{k_i} \\ &\quad \times r_{q-1}^{\sum_{i=1}^n k_i} (1-r_{q-1})^{q+(q-2)(\sum_{i=1}^{n-1} k_i)-k_n}, \end{aligned} \quad (\text{A6})$$

where the sum in $\{k_i\}$ sums for $k_0 = 1, k_1 = 0, 1, \dots, qk_0$, and $k_{i \geq 2} = 0, 1, \dots, (q-1)k_{i-1}$.

-
- [1] H. J. Kimble, *Nature* **453**, 1023 (2008).
[2] H. J. Briegel, W. Dür, J. I. Cirac, and P. Zoller, *Phys. Rev. Lett.* **81**, 5932 (1998).
[3] W. Dür, H. J. Briegel, J. I. Cirac, and P. Zoller, *Phys. Rev. A* **59**, 169 (1999).
[4] J. Calsamiglia, L. Hartmann, W. Dür, and H. J. Briegel, *Phys. Rev. Lett.* **95**, 180502 (2005).
[5] A. Acín, J. I. Cirac, and M. Lewenstein, *Nature Phys.* **3**, 256 (2007).
[6] S. Perseguers, J. I. Cirac, A. Acín, M. Lewenstein, and J. Wehr, *Phys. Rev. A* **77**, 022308 (2008).
[7] G. J. Lapeyre Jr., J. Wehr, and M. Lewenstein, *Phys. Rev. A* **79**, 042324 (2009).
[8] S. Perseguers, D. Cavalcanti, G. J. Lapeyre Jr., M. Lewenstein, and A. Acín, *Phys. Rev. A* **81**, 032327 (2010).
[9] S. Broadfoot, U. Dorner, and D. Jaksch, *Europhys. Lett.* **88**, 50002 (2009).
[10] S. Broadfoot, U. Dorner, and D. Jaksch, *Phys. Rev. A* **81**, 042316 (2010).
[11] S. Perseguers, *Phys. Rev. A* **81**, 012310 (2010).
[12] S. Broadfoot, U. Dorner, and D. Jaksch, *Phys. Rev. A* **82**, 042326 (2010).
[13] M. Cuquet and J. Calsamiglia, *Phys. Rev. Lett.* **103**, 240503 (2009).
[14] C. Moore and M. E. J. Newman, *Phys. Rev. E* **62**, 7059 (2000).
[15] M. E. J. Newman, S. H. Strogatz, and D. J. Watts, *Phys. Rev. E* **64**, 026118 (2001).
[16] S. N. Dorogovtsev, A. V. Goltsev, and J. F. F. Mendes, *Rev. Mod. Phys.* **80**, 1275 (2008).

- [17] M. Boguna, R. Pastor-Satorras, and A. Vespignani, *Phys. Rev. Lett.* **90**, 028701 (2003).
- [18] A. V. Goltsev, S. N. Dorogovtsev, and J. F. F. Mendes, *Phys. Rev. E* **78**, 051105 (2008).
- [19] M. E. J. Newman, *Phys. Rev. Lett.* **103**, 058701 (2009).
- [20] R. Cohen, K. Erez, D. ben-Avraham, and S. Havlin, *Phys. Rev. Lett.* **85**, 4626 (2000).
- [21] R. Albert, H. Jeong, and A.-L. Barabási, *Nature* **406**, 378 (2000).
- [22] R. Cohen, K. Erez, D. ben-Avraham, and S. Havlin, *Phys. Rev. Lett.* **86**, 3682 (2001).
- [23] B. Bollobás, *Random Graphs*, 2nd ed. (Cambridge University Press, Cambridge, 2001).
- [24] P. Bialas and A. K. Oles, *Phys. Rev. E* **77**, 036124 (2008).
- [25] M. A. Serrano, A. Maguitman, M. Boguñá, S. Fortunato, and A. Vespignani, *ACM Transactions on the Web (TWEB)* **1**, 10 (2007).
- [26] H. Wilf, *Generating Functionology*, 2nd ed. (AK Peters, London, 2006).
- [27] E. N. Gilbert, *Ann. Math. Stat.* **30**, 1141 (1959).
- [28] P. Erdős and A. Rényi, *Publ. Math. (Debrecen)* **6**, 290 (1959).
- [29] P. Erdős and A. Rényi, *Publ. Math. Inst. Hung. Acad. Sci.* **5**, 17 (1960).
- [30] D. J. Watts and S. H. Strogatz, *Nature* **393**, 440 (1998).
- [31] R. Albert, H. Jeong, and A.-L. Barabasi, *Nature* **401**, 130 (1999).
- [32] G. Vidal, *Phys. Rev. Lett.* **83**, 1046 (1999).
- [33] M. Zukowski, A. Zeilinger, M. A. Horne, and A. K. Ekert, *Phys. Rev. Lett.* **71**, 4287 (1993).
- [34] D. S. Callaway, M. E. J. Newman, S. H. Strogatz, and D. J. Watts, *Phys. Rev. Lett.* **85**, 5468 (2000).
- [35] M. Horodecki, P. Horodecki, and R. Horodecki, *Phys. Rev. A* **60**, 1888 (1999).
- [36] E. López, R. Parshani, R. Cohen, S. Carmi, and S. Havlin, *Phys. Rev. Lett.* **99**, 188701 (2007).
- [37] F. Verstraete and H. Verschelde, *Phys. Rev. Lett.* **90**, 097901 (2003).
- [38] A. Sen(De), U. Sen, C. Brukner, V. Bužek, and M. Żukowski, *Phys. Rev. A* **72**, 042310 (2005).
- [39] S. N. Dorogovtsev, J. F. F. Mendes, and A. N. Samukhin, *Nucl. Phys. B* **653**, 307 (2003).
- [40] J. Shao, S. V. Buldyrev, R. Cohen, M. Kitsak, S. Havlin, and H. E. Stanley, *Europhys. Lett.* **84**, 48004 (2008).
- [41] S. Perseguers, M. Lewenstein, A. Acín, and J. I. Cirac, *Nature Phys.* **6**, 539 (2010).